I. Rashidi
Department of Mechanical Engineering,
Ferdowsi University of Mashhad,
Mashhad, Iran

Ma. Pasandideh-Fard
Department of Mechanical Engineering,
Ferdowsi University of Mashhad,
Mashhad, Iran

Mo. Passandideh-Fard[1]
Department of Mechanical Engineering,
Ferdowsi University of Mashhad,
Mashhad, Iran

N. M. Nouri
School of Mechanical Engineering,
Iran University of Science and Technology,
Narmak, Tehran 16846, Iran

Numerical and Experimental Study of a Ventilated Supercavitating Vehicle

In this paper, the ventilated supercavities are studied both numerically and experimentally. A slender rod is considered as the solid body which has a sharp edged disk at the nose as a cavitator and special ports for air ventilation. The experiments are conducted in a recirculating water tunnel. The simulations are provided for two different algorithms in free-surface treatment, both using the VOF method but one using Youngs' algorithm in the advection of the free-surface and the other without. The comparison between numerical simulations and experiments show that the numerical method using Youngs' algorithm accurately simulates the physics of ventilated cavitation phenomena such as the cavity shape, the gas leakage and the re-entrant jet. [DOI: 10.1115/1.4027383]

1 Introduction

In this paper, the ventilated supercavities are studied both numerically and experimentally. When a large and continuous cavity covers the entire body of a submerged, moving vehicle the supercavitation occurs. This phenomenon makes a considerable reduction in the drag of the vehicle which in turn provides a substantial increase in the maximum speed. The supercavitation occurs at small cavitation numbers in the range of σ_c $2(p_\infty - p_c)/\rho U_\infty^2 < 0.1$. The supercavitation condition can be achieved in different ways. The natural supercavitation occurs when the free stream velocity is increased above a certain limit ($U_\infty > 45$ m/s at sea level, and increases with submersion depth, or p_∞). This phenomenon can also be achieved by decreasing the ambient pressure, p_∞ which is only feasible in cavitation tunnels. Increasing the cavity pressure, p_c, through ventilation of the cavity also results in supercavitation which is called artificial or ventilated supercavitation. Reichardt [1] was the first who studied supercavitation by artificially ventilating the flow around a body. The ventilated supercavitation is even applied to vehicles designed to travel at natural supercavitating conditions in order to reduce their drag and enable them to accelerate to conditions at which a natural supercavity is sustained. Fundamental dimensionless parameters for ventilated supercavities are the cavitation number, σ_c, and the Froude number, $Fr = U_\infty/(gd)^{1/2}$. At low Froude numbers, the gravitational effect becomes important which affects the shape of the cavity. In the design of a ventilated supercavitation condition, obtaining the amount of required ventilation gas in order to sustain a supercavity is the main objective. It is quantified by the dimensionless air entrainment coefficient, $CQ = Q/U_\infty d^2$.

The ventilated supercavity has been studied considerably in the literature by all means of experimental measurements and numerical simulations. Most experimental studies concentrated on cavitation over axisymmetric bodies focusing on the shape of the cavitation, the flow velocity, the pressure distributions and hydrodynamic coefficients of the models with cavitation. Savchenko et al. [2] obtained an empirical correlation for the shape and dimensions of an axisymmetric supercavitation. Hrubes [3] performed a high speed imaging of supercavitation for projectiles

underwater. Kuklinski et al. [4] investigated the instabilities of the ventilated cavity over dynamic test models. The effect of gravity and ventilation on the shape of supercavitation was studied by Savchenko [5] using water tunnel experiments. Feng et al. [6,7] investigated the fluctuation characteristics of natural and ventilated cavities over an axisymmetric body for cavitation numbers larger than 0.1. Zhang et al. [8] performed experiments on a slender body and compared the shape characteristics of natural and ventilated supercavities. Lee et al. [9] studied the effect of pitch angle for a ventilated supercavitating vehicle.

Numerical solution for simulation of cavitation has been used for the last few decades. Models based on the Navier–Stokes equations appeared in early 1990s. Among these models, homogeneous equilibrium is common to simulate both the natural and ventilated supercavities. In this method a single-fluid modeling approach is employed for both phases. The homogeneous equilibrium flow model assumes that there is no velocity slip between the phases at the cavity interface. Various models in this category differ in the relation that defines the variable density field. A precise and applicable approach is to solve an advection equation for the volume fraction of each phase and compute the density according to the volume fraction of the two phases. This approach is named transport-based equation model (TEM). Two main points should be considered regarding the TEM approach: (1) a solution strategy for the advection equation and (2) the selection of an appropriate mass transfer model (if the natural cavitation occurs). The solution of the advection equation has been performed in the literature by two methods: solving the phase transport equation and flow equations with the same numerical method [10–13]; and solving the phase transport equation using special interface tracking methods such as volume-of-fluid (VOF) technique in order to precisely predict the cavity interface [14,15]. In this technique, the interface is considered to be a discontinuity moving through the computational domain. Different VOF methods for tracking liquid–gas interfaces have been developed; the most known are simple line interface construction (SLIC) Noh and Woodward [16], Hirt–Nichols (Hirt and Nichols [17]) and Youngs' piecewise linear interface construction (PLIC) (Youngs [18]). In the SLIC and Hirt–Nichols methods, the free surface is approximated with piecewise constant and piecewise constant stair-stepped line segments, respectively. In Youngs' method, however, piecewise linear segments are used to reconstruct the interface. This method is therefore, more accurate. A review of the reported literature indicates that the VOF technique is in

---

Fig. 1 The schematic of the water tunnel

1- Test section
2- Diffuser
3- Water tank
4- Flow meter
5- Centrifugal pump
6- Honey comb and guide vane
7- Nozzle
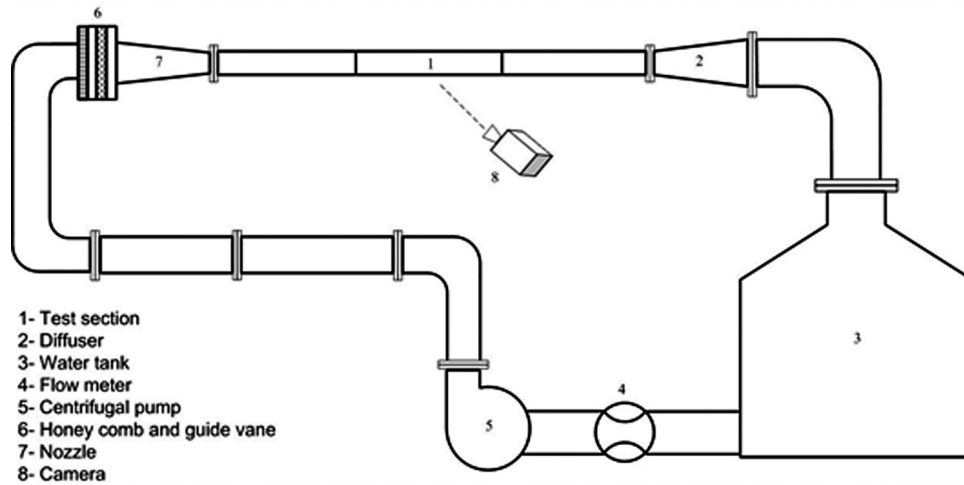8- Camera

accordance with natural cavitation physics and can accurately capture the shape and characteristics of a cavity [14,15]. Passandideh_Fard and Roohi [19] indicated that the VOF technique based on Youngs' method is a more accurate method to simulate the natural cavitation.

Numerical studies on ventilated supercavitation are rare in the literature. Jia et al. [20] determined the artificial ventilated cavity shape and provided a design reference for engineering applications. The shape of ventilated cavity and the drag of the underwater body were numerically simulated using a commercial code. Ji et al. [21] based on the Reynolds-Averaged Navier–Stokes (RANS) equations and mass transfer model proposed a three-component cavitation model to simulate the ventilated cavitating flow as well as natural cavitation. Pan et al. [22] presented a 3D numerical simulation of the periodically forced - pitching of the ventilated supercavitating vehicle. They solved the RANS equations for the ventilated cavitating flow field in a cavitation tunnel. Their solution was based on the finite volume method and the pressure-based segregate algorithm, in the framework of the mixture multiphase model, associated with a dynamic mesh. In the above studies, the phase transport equation and flow equations were solved by the same numerical method; no interface tracking was involved in the solution. As discussed above, the VOF technique based on Youngs' method is an accurate method to simulate the natural cavitation and is in accordance with cavitation physics. The main objective of this paper is to show that the VOF technique based on Youngs' method can also be used to simulate the 3D ventilated cavitation over an axisymmetric body. In addition, experiments are performed to validate the results obtained from the computations. Although ventilated supercavity has been extensively studied in the literature by means of experiments, many of these studies are related to supercavitation when the cavity closure is free. Much less data are available in the cases that cavity closes on a body. As a result, to examine the validity of numerical results presented in this paper for the cavity closure on the body in ventilated cavitation, experiments are also performed to obtain detailed information for the cavity shape, the gas leakage at the rear end of the cavity, the re-entrant jet, and the relationship between the three parameters of cavity length, air entrainment coefficient, and cavitation number.

2 Description of Experiment

The experiments were conducted in a water tunnel located at the Applied Hydrodynamics Laboratory of the Iran University of Science & Technology (IUST). A schematic of the water tunnel is displayed in Fig. 1. The tunnel is a recirculating, closed-jet facility with absolute pressure regulation and is capable of generating velocities up to 10 m/s. The test section which covers a space of 0.1 m in width, 0.2 m in height, and 4 m in length is fitted with observation windows on all four lateral sides. A gas separator of the tunnel allows for the removal of large quantities of air during ventilation experiments. The water tunnel is equipped with a data acquisition system and a single-shot photographic technique with 125 μs flash duration. It is also equipped with static pressure ports to measure the unsteady pressure in the cavity. Figure 2 shows a photograph of the model of the slender rod used in the water tunnel. The model which has a sharp edged disk at the nose as a cavitator and special ports for air ventilation is held fixed in the tunnel by a rear-supporting fixture.

3 Governing Equation

The governing equations for the 3D incompressible fluid flow are

$$\vec{\nabla}.\vec{V} = 0 \qquad (1)$$

$$\frac{\partial \vec{V}}{\partial t} + \vec{\nabla}.(\vec{V}\vec{V}) = -\frac{1}{\rho}\vec{\nabla}P + \frac{1}{\rho}\vec{\nabla}.(\vec{\tau} + \vec{\tau}_t) + \frac{1}{\rho}\vec{F}_b + \vec{g} \qquad (2)$$

where $\vec{V}$ is the velocity vector, P the pressure, F_b the body force acting on fluid, $\vec{g}$ the acceleration due to gravity and τ represents the Newtonian viscous stress tensor. The interface tracking between the phases is accomplished using an advection equation for the volume fraction of one of the phases as

$$\left[\frac{\partial}{\partial t}\left(\alpha_g\rho_g\right) + \vec{\nabla}\cdot\left(\alpha_g\rho_g\vec{V}\right)\right] = 0 \qquad (3)$$

where α_g and ρ_g are the volume fraction of the gas phase, respectively. The volume fraction equation will not be solved for the liquid phase; the liquid phase volume fraction (α_l) will be computed based on the following constraint:
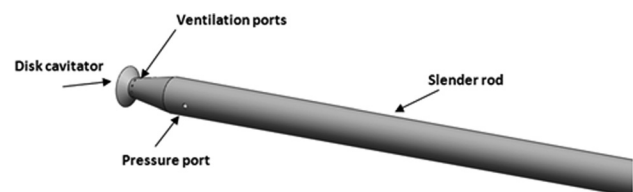

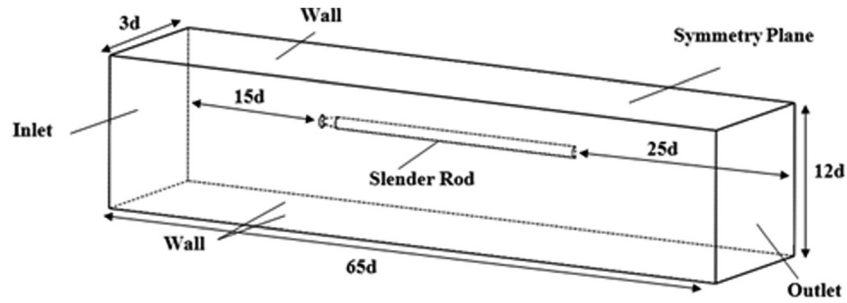**Fig. 2 The model used in the water tunnel**

Fig. 3 The computational domain and boundary conditions. The figure is not to scale.

$$\alpha_g + \alpha_l = 1 \qquad (4)$$

The density and viscosity of the mixture are calculated based on

$$\rho = \alpha_g \rho_g + (1 - \alpha_g)\rho_l, \quad \mu = \alpha_g \mu_g + (1 - \alpha_g)\mu_l \qquad (5)$$

The volume fraction equation was solved through an explicit time discretization scheme. The shape of interface is calculated using a geometric reconstruction scheme based on Youngs' PLIC algorithm discussed in detail elsewhere [19]. The set of the governing equations as described above along with the Reynolds stress model (RSM) as the turbulence model is solved using the ANSYS/FLUENT V12 software by a control volume approach.

The discretization of the pressure term is accomplished using the PRESTO! Scheme [23]. The pressure velocity coupling is performed by the SIMPLEC algorithm [23]. The second-order upwind scheme is applied to discretize the momentum equations and the first-order upwind scheme is used to discretize the turbulent equations. The QUICK scheme [24] is applied to discretize the advection equation (Eq. (3)). The linear system of discretized equations is solved by using a point implicit (Gauss–Seidel) linear equation solver together with the algebraic multigrid (AMG) method.

From the many simulations performed during the course of this study, the following procedure was taken in order to achieve convergence. The initial under-relaxation factors for the turbulence parameters, the pressure and the momentum were set at nearly 0.1; with converging the residuals this value was then gradually increased. For the two phase problems, an under-relaxation factor is also required for the volume fraction of one of the phases which was set at an initial value of 0.01; this value was then gradually increased to near one.

4 Computational Domain and Boundary Conditions

Figure 3 shows the computational domain including an underwater vehicle marked as "slender rod". The body has the following geometrical parameters: cavitator diameter d of 17 mm, the body diameter of 15 mm (0.88 d), and the body length of 400 mm (23.5 d). To maintain identical conditions in numerical simulations and experiments, the domain of the computation was considered to be the same as of the experimental test section. In order to save the computational cost and time, however, a plane of symmetry was assumed in the direction of the flow as seen in Fig. 3. It should be mentioned that although the physics of the cavitation phenomenon cannot be considered symmetric with respect to any plane, it is a typical routine in many simulations reported in the literature [20,21] to reduce the size of the computational domain by considering symmetry with respect to planes for which the flow shows less variations. The computational domain was 65 d in length, 12 d in height and 3 d in width; the experimental test section had the same size but only with 6d in width. The distance

between the domain inlet and the slender rod was 15 d, and that of the domain outlet and the end of the slender rod 25 d.

For ensuring computation accuracy, the structural grids have been used in total domain. The grid size is also progressively increased until the obtained simulation results are independent of size. This is done to justify the cell size used for the rest of the simulations presented afterwards. Finally, the total number of the grid is considered about 1,000,000. Figure 4 shows the structure grid near the body. Since the interaction between the near-wall flow and cavity should be taken into consideration, the mesh near the wall of test body is well refined so as to ensure the nondimensional normal distance from the wall, i.e., y^+, the value of y^+ at the wall surface of test body is smaller than 11.

The upstream velocity (V_∞) is considered at the inlet and the downstream pressure at the outlet is given a distribution of static pressure generated by gravity. The mass-flow-inlet boundary condition is used for the ventilation ports, and the total ventilation rate is Q. The no-slip boundary condition is applied at the walls of the tunnel and the body.

5 Results and Discussion

5.1 Model Validation. The shapes of the ventilated cavity from simulations are compared with those of the photographs in Figs. 5 and 6 for a value of CQ = 0.092 and 0.113, respectively. In each figure, the simulations are provided for two different algorithms in free-surface treatment, both using the VOF method but one using Youngs' algorithm in the advection of the free-surface (Figs. 5(b) and 6(b)) and the other without (Figs. 5(c) and 6(c)). The Froude number for both cases had a same value of Fr = 17. The figures show a good qualitative agreement between the
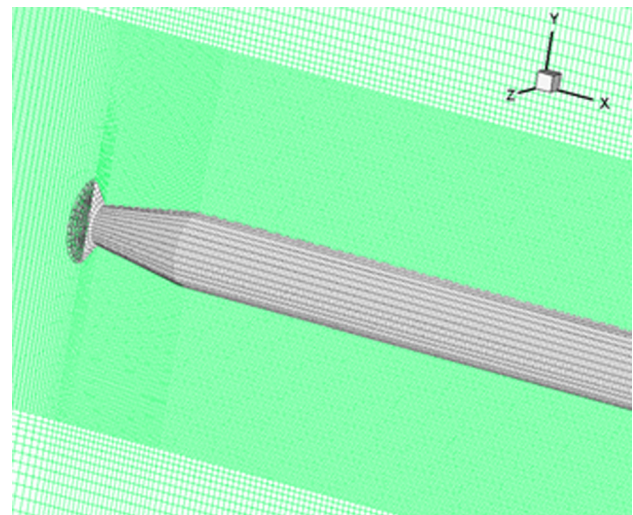

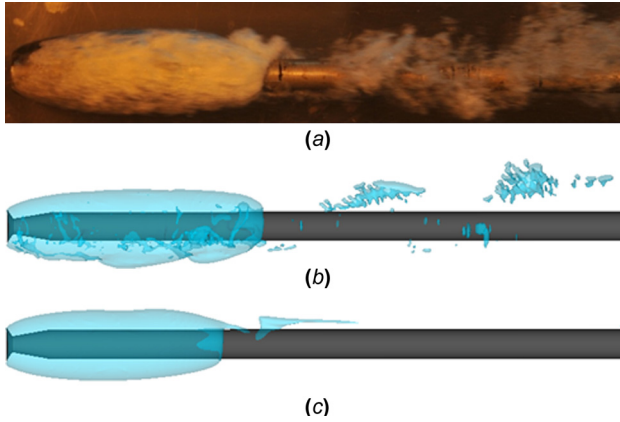**Fig. 4 The structure grid near the body**

Fig. 5 The shape of the ventilated cavity from (*a*) experiments, (*b*) simulations using Youngs' algorithm, and (*c*) simulations without Youngs' algorithm at an air entrainment coefficient of CQ = 0.092 and the Froude number of Fr = 17

experiments and the numerical results obtained using Youngs' algorithm. When this algorithm was not used in the simulations, however, the VOF method could not resolve the real physics of the phenomenon including the length of the cavity, gas leakage, and reentrant jet at the cavity closure. This comparison, therefore, confirms the validity of the Youngs' algorithm in modeling the ventilated cavitation by a correct prediction of both the shape and the length of the cavity. The experimental observations show that two principally different mechanisms of the gas leakage from the stable artificial cavities exist when the cavity closes on a solid body. At low values of air ventilation (CQ < 0.102) when the dimensionless cavity length is small (less than 10), the gravity effect is not significant. As a result, the cavity shape is close to that of the axisymmetric one, the cavity is filled by a foamy shape at the rear end leading to an unstable re-entrant jet and periodic vortices that evacuates the foam (Fig. 5(*a*)). When the air ventilation is increased, the length of the cavity grows, and it becomes well-ordered. In this case, the gravity influence will destroy the axisymmetric of ventilated cavity and cause the cavity characteristics at the rear end to tend upwards (Fig. 6(*a*)). As seen from Figs. 5(*b*) and 6(*b*), the numerical method using Youngs' algorithm accurately predicts the two regimes.

As shown above, the numerical method using Youngs' algorithm simulates the physics of ventilated cavitation phenomena, as well. In order to examine the validity of numerical method to predict the relationship between the three parameters of cavity length, air entrainment coefficient, and cavitation number, the variation
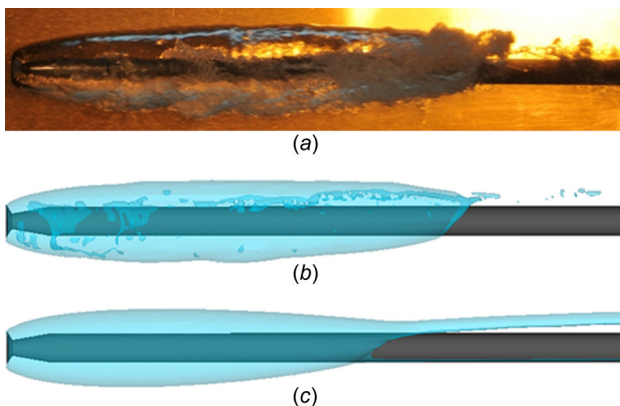

Fig. 6 The shape of the ventilated cavity from (*a*) experiments, (*b*) simulations using Youngs' algorithm, and (*c*) simulations without Youngs' algorithm at an air entrainment coefficient of CQ = 0.113 and the Froude number of Fr = 17
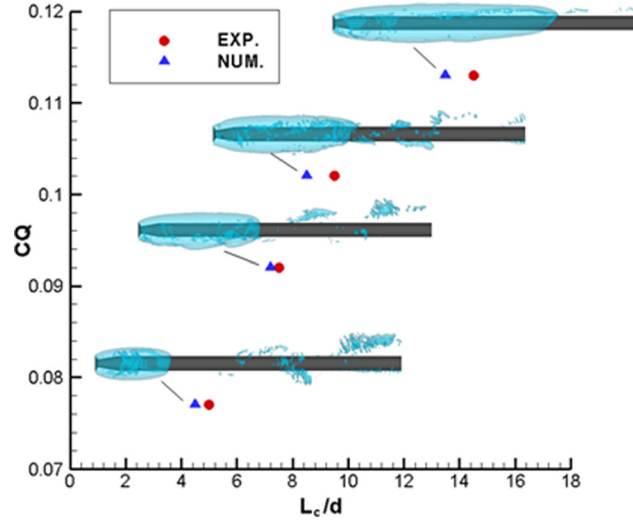

Fig. 7 The variation of the air entrainment coefficient (CQ) versus the dimensionless cavity length (L_c/d) from the numerical method using Youngs' algorithm and experiments for Fr = 17

of the air entrainment (CQ) against the dimensionless cavity length (L_c/d) and cavitation number (σ_c) is presented in Figs. 7 and 8, respectively. Both figures reveal a good agreement between the numerical results with those of the experiments. As observed, by increasing the value of CQ, the dimensionless length of the cavity is increased. Since the Froude number is assumed constant; therefore, the enlargement of the cavity causes the gravitational effect to be more pronounced for the case with larger CQ (Fig. 6). As CQ is increased, the value of pressure inside the cavity is also increased; therefore, since the Froude number is constant, the cavitation number is increased (Fig. 8).

5.2 The Re-Entrant Jet. An interesting phenomenon observed in experiments for ventilated cavitation is the extension of the re-entrant jet in upstream direction right up to the disk cavitator as shown in Fig. 9(*a*). As shown in Fig. 9(*b*) the numerical simulation also predicts the backward of liquid in the cavity. The qualitative comparison displayed in Fig. 7 indicates the ability of Youngs' algorithm in modeling the various features of ventilated
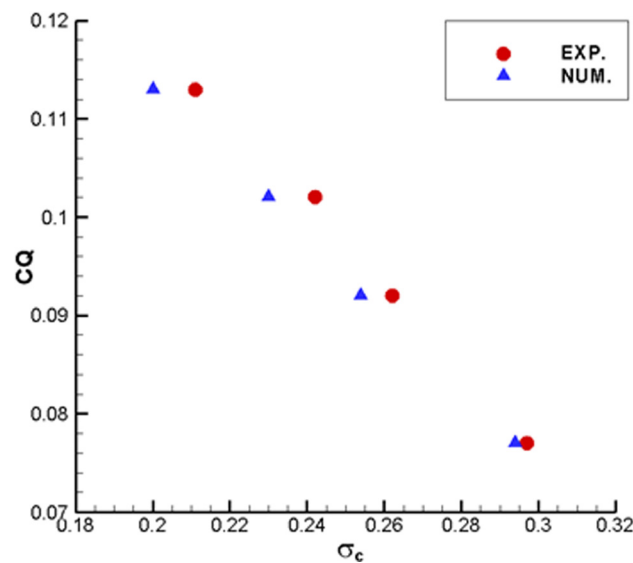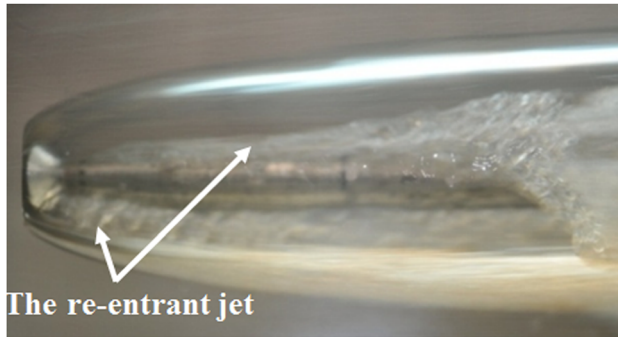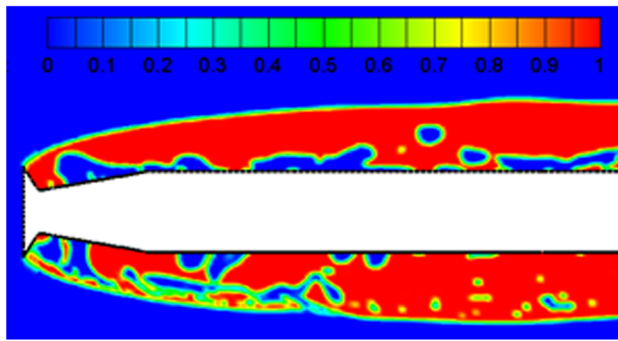

Fig. 8 The variation of the air entrainment coefficient (CQ) versus the cavitation number from the numerical method using Youngs' algorithm and experiments for Fr = 17

(a)

(b)

Fig. 9 The re-entrant jet in the ventilated cavitation from (a) experiments (where arrows point to the re-entrant jet) and (b) simulations using Youngs' algorithm (where a counter of the air volume fraction is shown)

cavitation. The re-entrant jet flow is better observed in Fig. 10 where a close-up of the cavity closure region is shown from both simulations and experiments. The numerical model provides more information regarding the re-entrant jet phenomenon. The flow inside the cavity for a case with CQ = 0.113 is displayed in Fig. 11. As seen from the figure, the re-entrant jet causes many air vortices inside the cavity.

5.3 The Transient Behavior of the Flow Inside the Cavity. The flow pressure distributions using the numerical method for the air entrainment of 0.102 and 0.113 are presented in Figs. 12
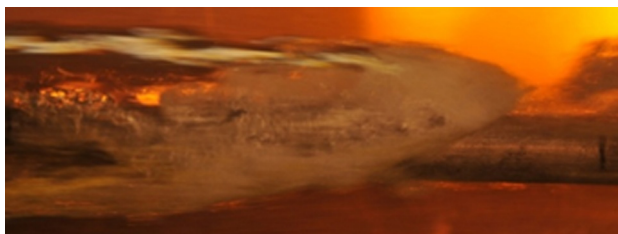
(a)

(b)

Fig. 10 The evacuation of the vortices at the rear end of the cavity from (a) experiments and (b) the simulations using Youngs' algorithm

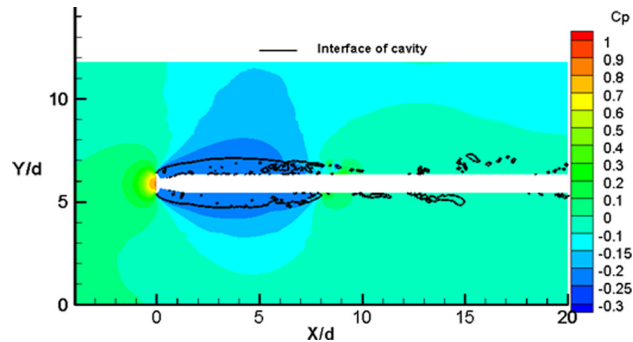**Fig. 11 The re-entrant jet inside the cavity**

Fig. 12 The pressure coefficient distributions from the numerical method using Youngs' algorithm for an air entrainment of 0.102 and Fr = 17. The cavity interface from the numerical method is also displayed in the figure.
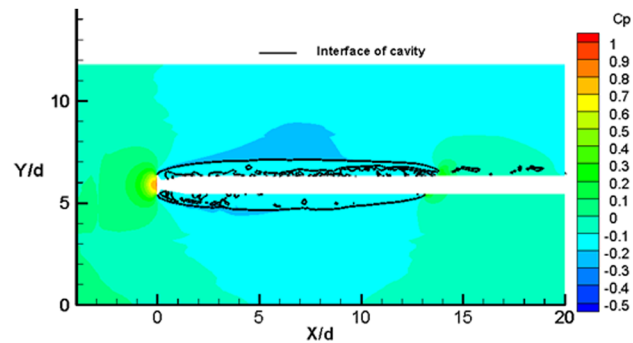

Fig. 13 The pressure coefficient distributions from the numerical method using Youngs' algorithm for an air entrainment of 0.113 and Fr = 17. The cavity interface from the numerical method is also displayed in the figure.

and 13, respectively. The cavity interface of the numerical method is also given in the same figure. It can be seen that inside the cavity, the pressure coefficient is constant at one moment. The re-entrant jet, however, causes the cavity pressure to vary in time, and as a result, the cavitation number varies with time as well. To show more clearly the transient behavior of the phenomenon, the variation of the cavitation number inside the cavity versus the time for CQ = 0.102 and CQ = 0.113 are plotted in Figs. 14 and 15, respectively. The mean value of the cavitation number is also seen in the figures. It should be mentioned that the value of the cavitation number from the numerical model presented in Fig. 8 are the mean value obtained from calculations. The unsteady behavior of the ventilated cavitation inside the cavity can also be seen in Figs. 16 and 17 where transparent views of the cavity at various time steps are shown. For a CQ of 0.102 where the dimensionless cavity length has nearly a constant value of 8.5 at various times, the re-entrant jet is responsible for different transient behavior of flow such as the cavity interface, the cavity detachment, and the flow inside the cavity. When CQ is increased, however, the unsteady characteristics of the flow are limited to the flow inside. As Fig. 17 shows, the cavity interface in this case remains nearly constant, and the cavity detachment is more ordered compared to that of Fig. 16.
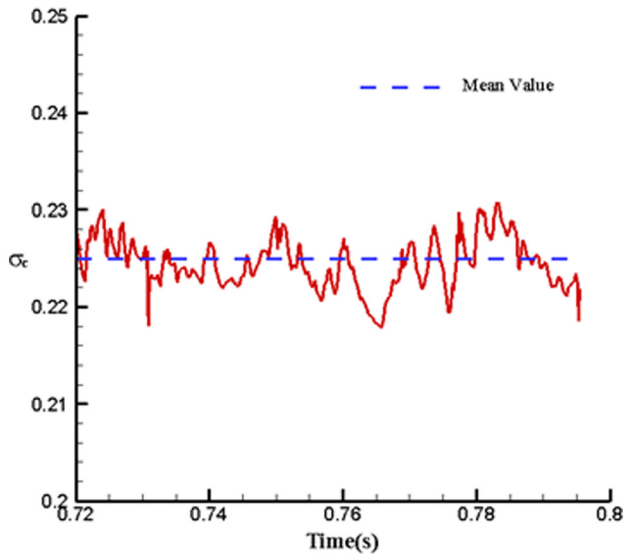
Fig. 14 The time variation of cavitation number inside the cavity for CQ = 0.102 and Fr = 17. The mean value of the cavitation number is also shown.
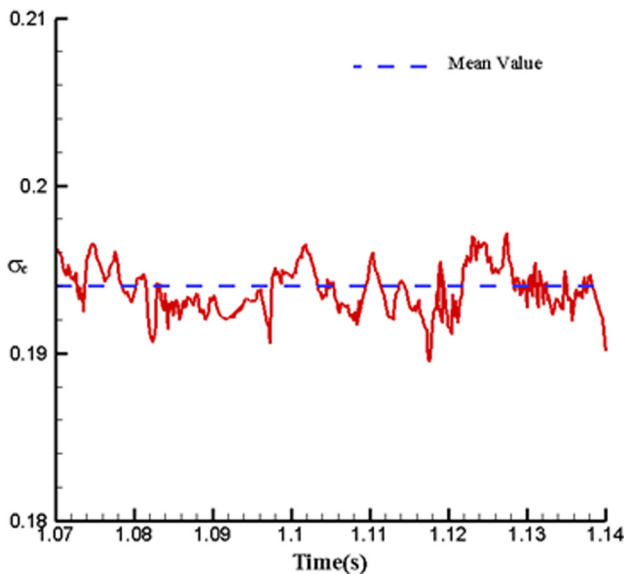

Fig. 15 The time variation of cavitation number inside the cavity for CQ = 0.113 and Fr = 17. The mean value of the cavitation number is also shown.
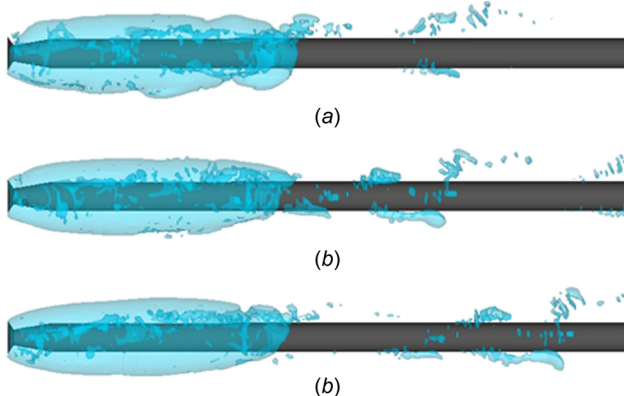

Fig. 16 The unsteady behavior of the ventilated cavitation for CQ = 0.102. The time interval between successive images is 0.01 s.
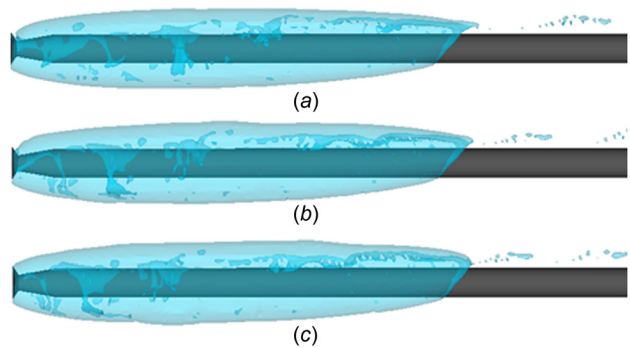

Fig. 17 The unsteady behavior of the ventilated cavitation for CQ = 0.113. The time interval between successive images is 0.01 s.

6 Conclusion

Ventilated supercavities were studied both numerically and experimentally. The experiments were conducted in a water tunnel located at the Applied Hydrodynamics Laboratory of the Iran University of Science & Technology (IUST). The model used to investigate was a slender rod which had a sharp edged disk at the nose as a cavitator and special ports for air ventilation. The simulations were conducted for two different algorithms in free-surface treatment, both using the VOF method but one using Youngs' algorithm in the advection of the free-surface and the other without. The comparison between numerical simulation and experiments showed that the numerical method using Youngs' algorithm accurately simulates the physics of ventilated cavitation phenomena such as the cavity shape, the gas leakage at the rear end of the cavity and the re-entrant jet. The numerical method also provided the relationship between the three parameters of cavity length, air entrainment coefficient and cavitation number as well. Simulations showed that inside the cavity, the pressure coefficient was constant at one moment. The re-entrant jet, however, caused the cavity pressure to vary in time, and as a result, the cavitation number varied in the time as well. It was found that the re-entrant jet is responsible for different transient behavior of flow such as the cavity interface, the cavity detachment, and the flow inside the cavity.

Acknowledgment

References

[1] Reichardt, H., 1946, "The Laws of Cavitation Bubbles at Axially Symmetrical Bodies in a Flow. Ministry of Aircraft Production (Great Britain)," Reports and Translations No. 766.
[2] Savchenko, Y. N., Vlasenko, Y. D., and Semenenko, V. N., 1999, "Experimental Study of High-Speed Cavitated Flows," Int. J. Fluid Mech. Res., **26**(3), pp. 365–374.
[3] Hrubes, J. D., 2001, "High-Speed Imaging of Supercavitation Underwater Projectiles," Exp. Fluids, **30**(1), pp. 57–64.
[4] Kuklinski, R., Henoch, C., and Cstano, J., 2001, "Experimental Study of Ventilated Cavities on Dynamic Test Model," 4th International Symposium on Cavitation, Pasadena, CA, Paper No. Cav01-B3-004.
[5] Savchenko, Y. N., and Semenenko, V. N., 1998, "The Gas Absorption Into Supercavity From Liquid-Gas Bubble Mixture," 3rd International Symposium on Cavitation, Grenoble, France, Vol. 2, pp. 49–53.
[6] Feng, X.-M., Lu, C.-J., and Hu, T.-Q., 2002, "Experimental Research on a Supercavitating Slender Body of Revolution With Ventilation," J. Hydrodyn., **14**(2), pp. 17–23.
[7] Feng, X.-M., Lu, C.-J., and Hu, T.-Q., 2005, "The Fluctuation Characteristics of Natural and Ventilated Cavities on an Axisymmetric Body," J. Hydrodyn., **17**(1), pp. 87–91.
[8] Zhang, X.-W., Wei Y.-J., and Zhang, J.-Z., 2007, "Experimental Research on the Shape Characters of Natural and Ventilated Supercavitation," J. Hydrodyn., **19**(5), pp. 564–571.

[9] Lee, Q.-T., Xue L.-P., and He, Y.-S., 2008, "Experimental Study of Ventilated Supercavities With a Dynamic Pitching Model," J. Hydrodyn., **20**(4), pp. 456–460.

[10] Wang, G., Senocak, I., Shyy, W., Ikohagi T., and Cao, S., 2001, "Dynamics of Attached Turbulent Cavitating Flows," Prog. Aerosp. Sci., **37**, pp. 551–581.

[11] Yuan, W., Sauer, J., and Schnerr, G. H., 2001, "Modeling and Computation of Unsteady Cavitation Flows in Injection Nozzles," J. Mech. Ind., **2**, pp. 383–394.

[12] Singhal, A. K., Athavale, M. M., Li, H., and Jiang, Y., 2002, "Mathematical Basis and Validation of the Full Cavitation Model," ASME J. Fluids Eng., **124**(3), pp. 617–624.

[13] Kunz, R. F., Boger, D. A., Stinebring, D. R., Chyczewski, T. S., Lindau, J. W., Gibeling, H. J., Venkateswaran, S., and Govindan, T. R., 2000, "A Preconditioned Navier–Stokes Method for Two-Phase Flows With Application to Cavitation," Comput. Fluids, **29**, pp. 849–875.

[14] Frobenius, M., Schilling, R., Bachert, R., and Stoffel, B., 2003, "Three-Dimensional Unsteady Cavitating Effects on a Single Hydrofoil and in a Radial Pump Measurement and Numerical Simulation," Proceedings of the 5th International Symposium on Cavitation (CAV2003), Osaka, Japan, Paper No. GS-9-004.

[15] Wiesche, S., 2005, "Numerical Simulation of Cavitation Effects Behind Obstacles and in an Automotive Fuel Jet Pump," Heat Mass Transfer, **41**(7), pp. 615–624.

[16] Noh, W. F., and Woodward, P. R., 1976, "SLIC (Simple Line Interface Calculation)," Lecture Notes in Physics, **59**, p. 330–340.

[17] Hirt, F. H., and Nichols, B. D., 1981, "Volume of Fluid (VOF) Method for the Dynamics of Free Boundaries," J. Comput. Physics, **39**, pp. 201–225.

[18] Youngs, D. L., 1984, "An Interface Tracking Method for a 3D Eulerian Hydrodynamics Code," Atomic Weapons Research Establishment (AWRE) Technical Report No. 44/92/35.

[19] Passandideh_Fard, M., and Roohi, E., 2008, "Transient Simulations of Cavitating Flows using a Modied Volume of Fluid VOF Technique," Int. J. Comput. Fluid Dyn., **22**(1–2), pp. 97–114.

[20] Jia, L.-P, Wang, C. Wei, Y.-J., Wang, H.-B., Zhang, J.-Z., and Yu, K.-P., 2006, "Numerical Simulation of Artificial Ventilated Cavity," J. Hydrodyn. **18**(3), pp. 273–279.

[21] Ji, B., and Luo, X.-W., 2010, "Numerical Investigation of the Ventilated Cavitating Flow Around an Under-Water Vehicle Based on a Three-Component Cavitation Model," J. Hydrodyn., **22**(6), pp. 753–759.

[22] Pan, Z.-C., Lu, C.-J., Chen, Y. and Hu, S.-L., 2010, "Numerical Study of Periodically Forced-Pitching of a Supercavitating Vehicle," J. Hydrodyn., **22**(5), pp. 899–904.

[23] Patankar, S. V., 1980, *Numerical Heat Transfer and Fluid*, Hemisphere, Washington, DC.

[24] Leonard, B. P., and Mokhtari, S., 1990, "ULTRA-SHARP Nonoscillatory Convection Schemes for High-Speed Steady Multidimensional Flow," NASA Lewis Research Center, Report No. NASA-TM-102568 (ICOMP-90-12),